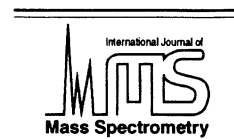




ELSEVIER

International Journal of Mass Spectrometry 212 (2001) 97–109



www.elsevier.com/locate/ijms

# Multidimensional separations of complex peptide mixtures: a combined high-performance liquid chromatography/ion mobility/time-of-flight mass spectrometry approach

Stephen J. Valentine<sup>1,\*</sup>, Manoj Kulchania, Catherine A. Srebalus Barnes, David E. Clemmer

*Department of Chemistry, Indiana University, Bloomington, Indiana 47405*

Received 17 April 2001; accepted 30 July 2001

## Abstract

High-performance liquid chromatography (HPLC) has been combined with high-resolution ion mobility separations and time-of-flight mass spectrometry (MS) for the analysis of complex biomolecular mixtures such as those that arise upon tryptic digestion of protein mixtures. In this approach, components in a mixture are separated using reversed phase HPLC. As mixtures of peptides exit the column, they are electrosprayed into an ion mobility/time-of-flight mass spectrometer. Mixtures of ions are separated based on differences in mobilities through a buffer gas, and subsequently dispersed by differences in mass-to-charge ( $m/z$ ) ratios in a mass spectrometer. The multidimensional approach is feasible because of the large differences in timescales of the HPLC (minutes), ion mobility (milliseconds), and time-of-flight (microseconds) techniques. Peak capacities for the two-dimensional liquid chromatography-ion mobility separations (LC-IMS) and three-dimensional LC-IMS-MS separations are estimated to be  $\sim 900$  to 1 200 and  $\sim 3.7$  to  $4.6 \times 10^5$ , respectively. The experimental apparatus and data acquisition considerations are described; data for a mixture of peptides obtained upon tryptic digestion of five proteins (albumin, bovine and pig; cytochrome c, horse; hemoglobin, dog and pig) are presented to illustrate the approach. (Int J Mass Spectrom 212 (2001) 97–109) © 2001 Elsevier Science B.V.

*Keywords:* Multidimensional separations; Ion mobility spectrometry; Proteomics; Chromatography

## 1. Introduction

We have recently coupled gas-phase ion mobility separations (IMS) with time-of-flight (TOF) mass spectrometry (MS) and developed a nested data ac-

quisition system that allows mobilities and mass-to-charge ( $m/z$ ) ratios for mixtures of ions to be determined from a single experimental sequence [1]. The method has several attractive features for analyzing mixtures, including: the ability to resolve sequence and structural isomers [2–6]; an overall reduction in the congestion of mass spectral peaks from electrospray ionization (ESI); simplification of charge state assignment based on peak positions in mobility families [7–9]; and a complementary means of assigning isomers (or sequences with nearly identical  $m/z$  ratios)

\* Corresponding author. E-mail: svalentine@beyondgenomics.com

<sup>1</sup>Current Address: Beyond Genomics, Inc., Waltham, Massachusetts 02451

Dedicated to R. Graham Cooks on the occasion of his sixtieth birthday.

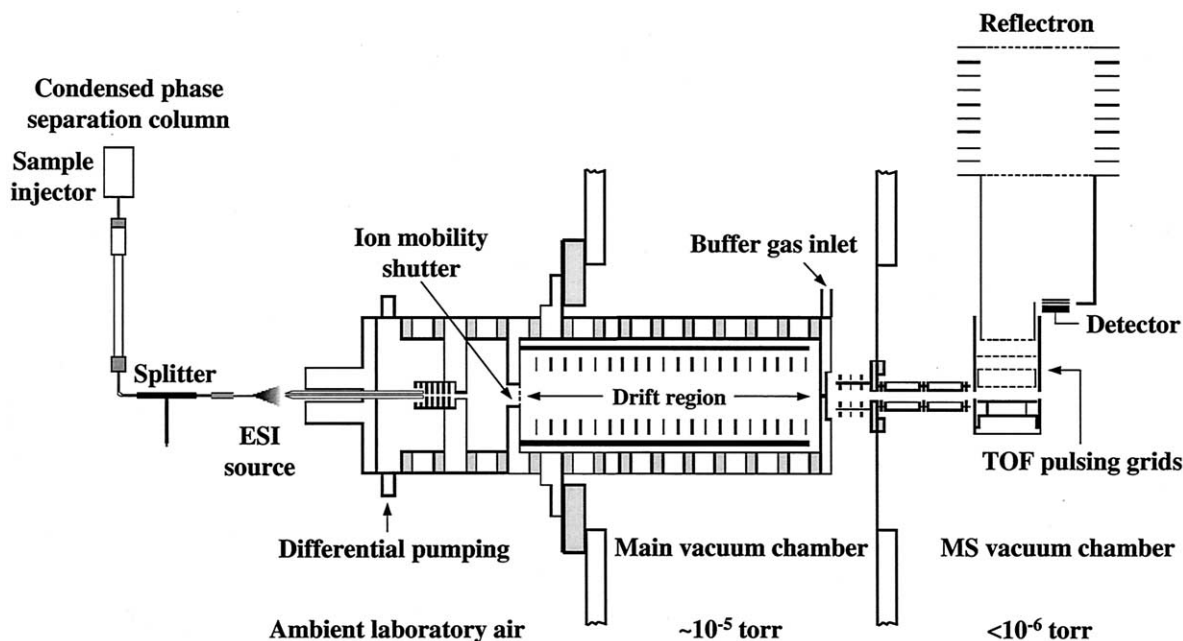


Fig. 1. Schematic diagram of the experimental apparatus used for multidimensional separations. The condensed phase separation is carried out using a commercial Waters HPLC. This instrument and the ESI source region reside outside a main vacuum chamber that houses the drift tube. The time-of-flight mass spectrometer and detector are housed in a separate chamber.

based on combined molecular modeling/mobility calculation methods [2,5,9] or predictions of mobilities based on intrinsic amino acid sizes [8,10]. In addition, the ms timescale of the mobility measurement is sufficiently short to allow the nested two-dimensional approach to be coupled to longer timescale condensed-phase separations -creating a multidimensional dispersion of components. In this paper we present the first description of such an approach -high performance-liquid chromatography (HPLC) followed by a nested IMS-MS detection. The method is illustrated by analyzing a mixture of tryptic peptides arising from digestion of five proteins (albumin, bovine and pig; cytochrome c, horse; hemoglobin, dog and pig).

Theory [11] and results from experiment [12] for two-dimensional separation strategies have been discussed previously. Peak capacities (associated with each dimension) for hybrid methods scale multiplicatively [11]; thus multidimensional separations are especially relevant for the analysis of complex mixtures. For example, two-dimensional gel electrophoresis, where mixtures of proteins are separated by

differences in mass along one dimension and charge along another, offers peak capacities of  $\sim 10^3$  to  $10^4$ . On-line methods involving a separation step coupled with MS provide a rapid and sensitive approach for directly identifying components in mixtures [13–17]. Additionally, the tremendous resolving power of high-resolution MS methods makes these well suited for complex systems [17].

## 2. Experimental

### 2.1. General

Traditional ion mobility/MS methods [18,19] including a number of recent instruments with biomolecular ion sources [19–23] and our nested ion mobility/time-of-flight methods have been discussed in detail previously [1,9]; only a brief description of methods and modifications that are specific to the three-dimensional separation is presented here. Fig. 1 shows a schematic diagram of the experimental appa-

ratus. An overview of the three-dimensional analysis is as follows. A mixture of peptides is injected onto a HPLC column. As components leave the column, they are electrosprayed into a high-resolution ion mobility instrument and separated based on differences in their gas-phase mobilities. Highly charged ions experience a greater drift force than singly charged ions and therefore usually exhibit relatively short drift times. For ions of the same charge (and similar mass) compact conformers have shorter drift times than more elongated structures. As ions exit the drift tube they are focused into the source region of the TOF mass spectrometer and dispersed by differences in  $m/z$  ratios. Because  $\mu\text{s}$  flight times in the evacuated flight tube and  $\text{ms}$  drift times in the high pressure drift tube are much shorter than the  $\sim 45$  min timescale of the HPLC separation, it is possible to record many nested two-dimensional drift (flight) time distributions as species elute from the column; accumulation of these data at varying retention times forms a three-dimensional dataset comprised of retention times, drift times, and flight times.

## 2.2. Preparation of mixtures

Cytochrome c (horse heart, 95%), serum albumin (bovine, 99% and pig, 99%), and hemoglobin (dog and pig) [24] are obtained from Sigma and used without further purification. Tryptic digests of each protein are generated by addition of 150  $\mu\text{L}$  of a 0.2 mg/mL trypsin (Sigma, sequencing grade) in 0.2 M ammonium bicarbonate (EM Science) to 0.5 mL of a 20 mg/mL solution of each protein. After incubation for 20 h at 37 °C, the trypsin is filtered from the digest using a microconcentrator (Microcon 10, Amicon, Inc.) and the peptides that remain are lyophilized. A mixture is prepared by combining 2.0 mg of each of the digested protein samples in 1.0 mL of water. For direct infusion experiments, a 1.0 mL aliquot of the mixture is diluted with 1.0 mL of acetonitrile and 40  $\mu\text{L}$  of acetic acid. The sample is then electrosprayed using a flow rate of 1.3  $\mu\text{L}/\text{min}$ .

## 2.3. High-performance liquid chromatography/electrospray ionization interface

Peptides are separated on a  $4.6 \times 150$  mm C<sub>18</sub> column (5  $\mu\text{m}$  particle diameter; 300 Å pore size) from

Phenomenex using a Waters (Model 600) HPLC. A gradient elution using a water/acetonitrile solvent system (each with 0.1% formic acid) is used. For HPLC studies, peptides are detected by a Waters 2487 dual  $\lambda$  absorbance detector at 214 nm. For multidimensional separation experiments the flow volume is reduced by a factor of 60 (by a standard splitting approach) prior to ESI. A flow rate of 0.75 ml/min is used for the HPLC separation and the solvent system is stepped from 90:10 (H<sub>2</sub>O:Acetonitrile) to 35:65 over 55 min. Ions are electrosprayed at atmospheric pressure into a differentially pumped desolvation region through a 0.10 cm entrance orifice and introduced into the drift tube as described previously [25].

## 2.4. Mobility/time-of-flight mass spectrometry measurements

Mobility experiments are initiated by gating a short pulse (50–400  $\mu\text{s}$ ) of ions into the front of the drift tube. The drift tube is 58.23 cm long with a 100  $\mu\text{m}$  diameter exit aperture and is operated at 300 K using an applied drift field of 171.7 V cm<sup>-1</sup> and  $\sim 150$  Torr of He buffer gas. The time for ions to travel through the buffer gas ( $t_d$ ) depends upon their mobilities through the gas. The drift force that an ion experiences is proportional to its charge. High charge states usually have higher mobilities than low charge states. An exception to this occurs when highly charged ions adopt extended conformations in order to reduce coulomb repulsion. These high-cross section ions can have lower mobilities than lower charge states (with compact conformations). Derivations of experimental mobilities from drift times requires a correction associated with the time that ions spend in other portions of the instrument [19]. For the range of ions studied in the present experiments, these corrections are small ( $\sim 80$ – $120$   $\mu\text{s}$ ).

The resolving power,  $t_d/\Delta t$  (in which  $\Delta t$  is the full width at half maximum of the peak), of ion mobility experiments is given by [26]

$$\frac{t_d}{\Delta t} = \left[ \frac{LEze}{16k_B T \ln 2} \right]^{1/2} \quad (1)$$

where  $E$  is the electric field,  $L$  is the length of the drift tube, and  $T$  is the buffer gas temperature. The vari-

ables  $z$ ,  $e$ , and  $k_B$  are the ion charge state, the charge of an electron, and Boltzmann's constant, respectively. Several groups have reported high resolving powers,  $t_d/\Delta t > 80$  [6,25,27]. In our current arrangement, typical values of  $t_d/\Delta t \approx 120$ –150 are obtained for singly charged ions. It is possible to obtain higher resolving powers for higher charge states; we have reported resolving powers of  $\sim 260$  for +4 ions [6]. As a comparison, values of  $t_d/\Delta t = 100$ , 200, and 300 correspond to  $5.54 \times 10^4$ ,  $2.22 \times 10^5$ , and  $4.99 \times 10^5$  theoretical plates [28].

As ions exit the drift tube they are focused into the source region of reflectron geometry TOF mass spectrometer that is housed in a separate vacuum chamber. Typically the pressure in this region is  $\sim 1 \times 10^{-6}$  Torr. The resolving power of the mass spectrometer is typically 1200 to 2000 ( $m/\Delta m$ , where  $\Delta m$  is determined at half maximum) for a single isotopic peak of a singly charged ion having a mass of  $\sim 300$ –1200. Nested measurements of drift times and flight times ( $t_f$ ) are carried out using a synchronous pulse sequence and data acquisition system that has been described in detail previously [1]. We refer to two-dimensional ion mobility/time-of-flight datasets as nested drift time and flight time data - denoted as  $t_d(t_f)$ ; unless otherwise noted, drift and flight times are reported in units of ms and  $\mu$ s, respectively [1].

### 2.5. Acquisition of retention time, drift time, flight time datasets

Data for the three dimensional separations shown below are recorded as follows. After an initial delay of 12.2 min, 25 nested  $t_d(t_f)$  datasets, each 127 s in duration, are recorded sequentially. The 127 s acquisition time is chosen after a series of preliminary studies. Shorter acquisition times allow a greater number of nested  $t_d(t_f)$  windows to be recorded during the LC separation. However, peaks within individual nested  $t_d(t_f)$  windows are often less intense because ion intensity for more of the peaks is accumulated in two adjacent  $t_d(t_f)$  windows. Additionally, each two-dimensional  $t_d(t_f)$  distribution requires 3.0 s ( $\sim 2.3\%$  of the total 130 s window time) to save to the computer. Thus, when substantially shorter acquisi-

tion times are used, a significant fraction of ions is missed during the time required to save the data. To improve the speed and sensitivity of acquisition, data are sampled over narrow drift and flight time ranges of 14.000–22.448 ms and 19.400–30.500  $\mu$ s, respectively. This flight time range corresponds to a  $m/z \approx 390$ –920 range. Intensities along the drift and flight time axes are binned into 256 windows (each 33  $\mu$ s in duration) and 2 220 windows (each 5 ns in duration), respectively. Flight times are converted to  $m/z$  ratios by use of a calibration curve determined for individual tryptic digest mixtures having peaks across the  $m/z$  range of interest. Plots of the data are created using the MATLAB software [29].

## 3. Results and discussion

### 3.1. Nested $t_d(t_f)$ data for the five protein tryptic peptide mixture

Fig. 2 shows a nested  $t_d(t_f)$  dataset obtained upon electrospraying the complete mixture of tryptic peptides from the albumin (bovine and pig), cytochrome c (horse), and hemoglobin (dog and pig) proteins. Complete digestion would result in 187 peptides; of these 145 would be expected to form  $[M + H]^+$  and  $[M + 2H]^{2+}$  ions that fall within the  $m/z = 390$  to 920 range. Ninety-eight peaks and many additional small features are observed over this range. As discussed previously [7–10], the two-dimensional approach substantially reduces spectral congestion associated with the mass spectrum. Additionally, most peaks fall along charge state families. Based on our previous work it is straightforward to assign the  $[M + H]^+$  and  $[M + 2H]^{2+}$  families. Analysis of several peaks in each of these families corroborates these assignments. For example,  $m/z$  ratios derived for peaks 1(h) at 17.30(22.409), 1(m) at 18.79(24.280), and 1(ae) at 22.31(28.130) indicate that these peaks correspond to singly protonated GTFAK, GITWK, and LVTDLTK peptides, respectively. Peaks 2(e) at 14.47(23.033), 2(g) at 15.63(23.633), and 2(w) at 18.52(29.183) in the  $[M + 2H]^{2+}$  family are due to the doubly protonated LHVDPENFK, VVAGVANALAHK, and LGHDFNPVQAAFQK

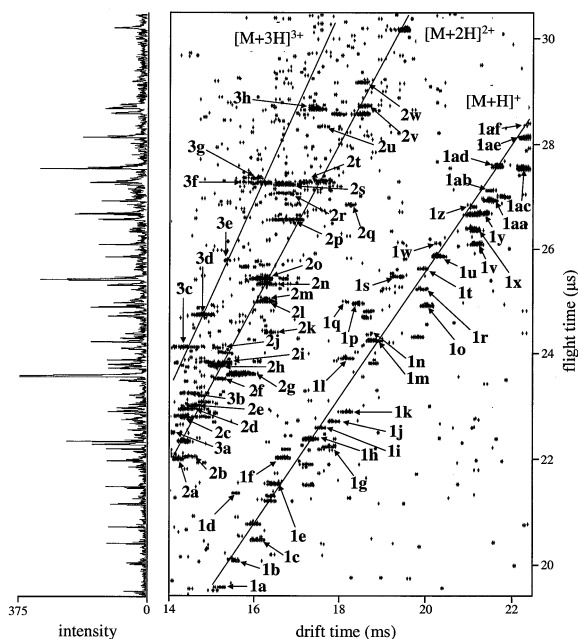


Fig. 2. Nested  $t_d(t_f)$  distribution for a mixture of ions produced by direct electrospray of a tryptic peptide mixture from digestion of dog and pig hemoglobin, bovine and pig albumin, and cytochrome c. The points represent regions in the two-dimensional array where ions have been observed. These data are displayed using a baseline cutoff of 2 such that any windows with fewer than two ion hits are not shown. The solid lines in the two-dimensional plot indicate the position of the  $[M + H]^+$ ,  $[M + 2H]^{2+}$ , and  $[M + 3H]^{3+}$  charge state families. The numbers and letters are used to label peaks and correspond to the assignments given in Table 1. To the left we have shown a mass spectrum that is obtained by summing the intensities at a given flight time across all drift time windows. These data were acquired using a drift field of  $171.7 \text{ V cm}^{-1}$  using a 300 K helium pressure of 150.3 Torr. The data were acquired in  $\sim 100$  min.

peptides, respectively. A complete summary of the data and assignments of peaks is given in Table 1.

A few peaks having higher mobilities than ions in the  $[M + 2H]^{2+}$  family are also observed. Peaks 3(a)–3(h) correspond to larger  $[M + 3H]^{3+}$  peptides. Although we have pointed out several triply charged ions previously [9] we have not reported a +3 family prior to this work.  $[M + 3H]^{3+}$  fragments generally arise from incomplete tryptic digestion or from sequences that contain a relatively basic histidine residue. The large size of the mixture of peptides from digestion of five proteins allows the  $[M + 3H]^{3+}$  family to be clearly discerned. The +3 family exhibits

a wider range of mobilities (for similar  $m/z$  ions) than is observed in the  $[M + H]^+$  and  $[M + 2H]^{2+}$  families because many +3 ions adopt highly extended conformations in order to minimize coulomb repulsion between charge sites. This is especially true for small peptides where charge repulsion is distributed over fewer residues. We have observed several cases in which highly extended  $[M + 3H]^{3+}$  conformations fall along the  $[M + 2H]^{2+}$  charge state family (e.g. peaks 3(a) and 3(b) in Fig. 2).

The summary  $t_d(t_f)$  data and assignments in Table 1 show that 60 of the 98 resolved peaks can be assigned to fragments that are expected from digestion of the five proteins. The assigned fragments constitute 23.7%, 14.8%, 51.0%, 39.0%, and 60.3% of the primary sequences of albumin (bovine), albumin (pig), cytochrome c (horse), hemoglobin (dog), and hemoglobin (pig), respectively. The relative ordering of the sequence coverage is roughly consistent with the concentrations of the peptide fragments that are expected upon digestion of equal masses of each of the parent proteins.

Although the two-dimensional method allows many similar  $m/z$  peaks to be resolved, spectral congestion in the  $t_d(t_f)$  dataset is still sufficiently high that some peaks cannot be unambiguously assigned. For example, peak 1(y) centered at 21.22(26.667) is somewhat broader in both the mobility and  $m/z$  dimensions than most other peaks in the  $[M + H]^+$  family. Three peptides AACLLPK, NLDNLK, and VADALTK having calculated  $[M + H]^+$   $m/z$  ratios of 715.4, 716.4, and 717.4, respectively, could be present. The small differences in mobilities and  $m/z$  ratios of these singly charged sequences are such that these peaks in Fig. 2 are not entirely resolved along either the drift or flight time dimension. Below, we show that the three-dimensional approach allows such features to be resolved.

### 3.2. Multidimensional high-performance liquid chromatography-ion mobility-mass spectrometry separation

Fig. 3 shows a representation of the three-dimensional HPLC-IMS-MS separation. Along the retention

Table 1  
Flight times, masses, and assignments of tryptic digest peptides<sup>a</sup>

[M+H] <sup>+</sup> family					[M+2H] <sup>2+</sup> family				
peak label	t <sub>r</sub> (mass) <sup>b</sup>	calcd mol wt <sup>c</sup>	assignment <sup>d</sup>	source <sup>e</sup>	peak label	t <sub>r</sub> (mass) <sup>b</sup>	calcd mol wt <sup>c</sup>	assignment <sup>d</sup>	source <sup>e</sup>
1a	19.591 (404.6)	403.2	S <sup>452</sup> LGK <sup>455</sup> *	al_bovine		21.301 (474.7)	946.6	G <sup>6</sup> KKIFVQK <sup>13</sup>	cytc
1b	20.104 (425.5)	423.2	N <sup>339</sup> YK <sup>341</sup>	al_pig		21.457 (481.2)	959.5	E <sup>210</sup> KVLASSAR <sup>218</sup>	al_bovine
1c	20.491 (441.2)	438.2	Y <sup>434</sup> TR <sup>436</sup>	al_bovine	2a	22.026 (505.3)	1009.5	Q <sup>411</sup> NCELFEK <sup>418</sup> *	al_pig
1d	21.380 (478.0)	477.2	E <sup>335</sup> VCK <sup>338</sup> *	al_pig	2b	22.069 (507.1)	1013.6	Q <sup>549</sup> TALVELLK <sup>557</sup> *	al_bovine,pig
1e	21.556 (485.4)	486.3	N <sup>407</sup> LIK <sup>410</sup> *	al_pig		22.772 (537.5)	1071.6	F <sup>398</sup> QPLVDEPK <sup>406</sup>	al_pig
1f	22.047 (506.3)	507.3	F <sup>227</sup> GER <sup>230</sup>	al_bovine,pig	2c	22.851 (540.9)	1078.6	V <sup>67</sup> LNSFSDGLK <sup>76</sup> *	hb_dog
1g	22.263 (515.3)	515.3	Q <sup>543</sup> IKK <sup>546</sup>	al_bovine,pig	2d	22.974 (546.3)	1091.6	T <sup>8</sup> NIKSTWVK <sup>16</sup> *	hb_dog
1h	22.409 (521.7)	522.3	G <sup>83</sup> TFVK <sup>87</sup>	hb_dog,pig	2e	23.033 (550.3)	1097.5	L <sup>96</sup> HVDPENFK <sup>104</sup> *	hb_dog
1i	22.623 (531.0)	531.3	A <sup>12</sup> AWGK <sup>16</sup>	hb_pig	2f	23.549 (571.7)	1141.7	K <sup>546</sup> QTALVELLK <sup>555</sup> *	al_pig
1j	22.741 (536.1)	536.3	F <sup>157</sup> WGK <sup>160</sup> *	al_bovine,pig	2g	23.633 (575.5)	1148.7	V <sup>133</sup> VAGVANALAHK <sup>144</sup> *	hb_dog,pig
1k	22.931 (544.4)	544.3	V <sup>101</sup> ASLR <sup>105</sup>	al_bovine	2h	23.788 (582.3)	1162.6	L <sup>66</sup> VNELTEFAK <sup>75</sup> *	al_bovine
1l	23.942 (589.4)	589.3	A <sup>152</sup> DEKK <sup>156</sup> *	al_bovine	2i	23.845 (585.0)	1167.6	T <sup>28</sup> GPNLHGLFGR <sup>38</sup> *	cytc
1m	24.280 (604.7)	603.3	G <sup>56</sup> TTWK <sup>60</sup> *	cytc	2j	24.146 (599.3)	1196.6	D <sup>337</sup> VCKNYQEAQ <sup>346</sup> *	al_bovine
1n	24.390 (609.6)	608.3	A <sup>524</sup> FDEK <sup>528</sup>	al_bovine		24.294 (605.0)	1206.7	K <sup>66</sup> VLSFSDGLK <sup>76</sup>	hb_dog
1o	24.943 (635.0)	633.4	I <sup>9</sup> FVQK <sup>13</sup> *	cytc	2k	24.439 (611.9)	1220.7	K <sup>66</sup> VLQSFSDGLK <sup>76</sup> *	hb_pig
1p	24.982 (636.8)	635.3	S <sup>12</sup> TWVK <sup>16</sup> *	hb_dog		24.614 (619.9)	1237.7	A <sup>57</sup> HGQKVADALTK <sup>68</sup>	hb_pig
1q	24.390 (639.6)	638.4	V <sup>60</sup> KAHGK <sup>65</sup>	hb_dog,pig		24.752 (626.2)	1248.6	F <sup>35</sup> KDLGEEHFK <sup>44</sup>	al_bovine
1r	25.262 (649.9)	648.3	I <sup>205</sup> ETMR <sup>209</sup> *	al_bovine	2l	25.025 (638.8)	1273.6	F <sup>33</sup> KDLGEQYFK <sup>42</sup> *	al_pig
1s	25.500 (661.0)	659.3	T <sup>490</sup> PVSEK <sup>495</sup>	al_bovine,pig	2l	25.028 (638.9)	1273.7	L <sup>31</sup> LVVYPWTQR <sup>40</sup> *	hb_pig
1t	25.651 (668.1)	666.4	I <sup>203</sup> EHLR <sup>207</sup>	al_pig	2m	25.071 (641.0)	1278.7	F <sup>128</sup> LANVSTVLTSK <sup>139</sup> *	hb_pig
1u	25.882 (679.0)	677.4	Y <sup>74</sup> IPGTK <sup>79</sup> *	cytc	2n	25.356 (654.2)	1304.7	H <sup>402</sup> LVDEPQNLIK <sup>412</sup> *	al_bovine
1v	26.115 (690.1)	688.4	A <sup>236</sup> WSVAR <sup>241</sup>	al_bovine	2o	25.451 (658.7)	1313.7	V <sup>18</sup> NVDEVGGEALGR <sup>30</sup> *	hb_dog,pig
1w	26.115 (690.4)	688.4	V <sup>210</sup> LTSAAK <sup>216</sup>	al_pig	2p	26.579 (712.4)	1421.7	V <sup>17</sup> GGQAGAHGAEALER <sup>31</sup> *	hb_pig
1x	26.363 (702.0)	700.4	L <sup>451</sup> GLVGSR <sup>457</sup> *	al_pig		26.815 (723.8)	1444.8	F <sup>156</sup> WGKYLEIAR <sup>167</sup>	al_bovine,pig
1y	26.667 (716.6)	714.4	A <sup>196</sup> ACLLPK <sup>202</sup> *	al_pig	2q	26.858 (725.9)	1448.8	V <sup>133</sup> VAGVANALAHKYH <sup>146</sup>	hb_dog,pig
1y	26.667 (716.6)	715.4	N <sup>77</sup> LDNLK <sup>82</sup> *	hb_dog		26.934 (729.6)	1456.9	A <sup>233</sup> LKAWSVARLSQK <sup>245</sup>	al_bovine
1y	26.667 (716.6)	716.4	V <sup>62</sup> ADALTK <sup>68</sup> *	hb_pig	2r	27.074 (736.4)	1469.7	T <sup>40</sup> GQAPGFTYTDANK <sup>53</sup> *	cytc
1z	26.815 (723.8)	724.3	C <sup>581</sup> CAADDK <sup>587</sup> *	al_bovine		27.171 (741.1)	1478.8	L <sup>421</sup> GEYGFQNALIVR <sup>433</sup>	al_bovine,pig
1aa	26.936 (729.7)	728.4	V <sup>1</sup> LSPADK <sup>7</sup>	hb_dog	2s	27.248 (744.9)	1486.7	I <sup>17</sup> GGHAGDYGGEALDR <sup>31</sup> *	hb_dog
1ab	27.137 (739.9)	738.4	H <sup>77</sup> LDNLK <sup>82</sup>	hb_pig	2t	27.295 (747.2)	1494.7	E <sup>61</sup> ETLMEYLENPK <sup>72</sup> *	cytc
1ac	27.540 (759.3)	758.5	I <sup>255</sup> VTDLAK <sup>261</sup> *	al_pig	2t	27.295 (747.2)	1494.8	V <sup>436</sup> PQVSTPTLVEVAR <sup>449</sup> *	al_pig
1ad	27.580 (761.3)	761.5	K <sup>8</sup> IFVQK <sup>13</sup> *	cytc		28.336 (799.0)	1594.9	H <sup>361</sup> PEYAVSVLLRLAK <sup>374</sup>	al_bovine
1ae	28.130 (788.7)	788.5	L <sup>257</sup> VTDLTK <sup>263</sup> *	al_bovine	2u	28.349 (800.3)	1597.8	K <sup>39</sup> TGQAPGFTYTDANK <sup>53</sup> *	cytc
1af	28.710 (818.0)	816.5	S <sup>452</sup> LGKVGTR <sup>459</sup>	al_bovine	2v	28.734 (819.8)	1635.3	heme-C <sup>14</sup> AQCHTVEK <sup>22</sup> *	cytc
	28.792 (822.2)	822.4	E <sup>67</sup> VTEFAK <sup>73</sup>	al_pig		29.117 (838.7)	1674.9	G <sup>23</sup> GKHKTGPNLHGLFGR <sup>38</sup>	cytc
					2w	29.183 (842.8)	1684.8	L <sup>118</sup> GHDFNPNVQAAFQK <sup>132</sup> *	hb_pig

(continued on next page)

Table 1  
(continued)

[M+3H] <sup>3+</sup> family					
peak label	t <sub>f</sub> (mass) <sup>b</sup>	calcd mol wt <sup>c</sup>	assignment <sup>d</sup>	source <sup>e</sup>	
3a	22.529 (526.9)	1577.6	E <sup>267</sup> CCHGDLLECADDR <sup>280</sup> *	al_bovine.pig	
	22.678 (533.4)	1597.8	K <sup>399</sup> TGQAPGFTYTDANK <sup>53</sup>	cytc	
	23.107 (552.1)	1655.8	Y <sup>284</sup> ICENQDTISTK <sup>297</sup>	al_pig	
3b	23.274 (559.5)	1674.9	G <sup>23</sup> GKHKTGPNLHGLFGR <sup>38</sup> *	cytc	
	23.334 (562.2)	1684.8	L <sup>118</sup> GHDFNPVQAAFQK <sup>132</sup>	hb_pig	
	23.925 (588.6)	1764.9	D <sup>345</sup> VFLGTFLYEYSRR <sup>358</sup>	al_pig	
3c	24.153 (598.9)	1792.9	T <sup>41</sup> YFPHFDLSPGSAQVK <sup>56</sup> *	hb_dog	
3d	24.767 (626.9)	1875.9	T <sup>41</sup> YFPHFNLSHGSDQVK <sup>56</sup> *	hb_pig	
	24.939 (634.8)	1899.0	L <sup>421</sup> GEYGFQNALIVRYTR <sup>436</sup>	al_bovine	
3e	25.811 (675.9)	2024.2	K <sup>437</sup> VPQVSTETLVEVSRSLGK <sup>455</sup>	al_bovine	
	25.991 (684.2)	2047.9	F <sup>41</sup> FDSFGDLSTPDVMSNAK <sup>61</sup>	hb_dog	
3f	27.283 (746.6)	2236.1	A <sup>69</sup> VGHLDLPGALSALSDDLHAHK <sup>90</sup> *	hb_pig	
	27.324 (748.6)	2241.2	S <sup>9</sup> LVSGLWGVNVDEVGGEALGR <sup>30</sup>	hb_dog	
3g	27.367 (751.4)	2251.1	R <sup>316</sup> DELPADLNPLEHDFVEDK <sup>344</sup> *	al_pig	
3h	28.670 (816.0)	2444.2	V <sup>17</sup> G <sub>2</sub> QAGAHGAEALERMFLGFPT <sub>2</sub> K <sup>40</sup> *	hb_pig	

<sup>a</sup>Peaks assigned in Fig. 2. No assignment indicates the peaks were not observed in the two-dimensional experiment but were observed in the three-dimensional experiment.

<sup>b</sup>Measured flight times (t<sub>f</sub>) in (μs). Masses for [M+H]<sup>+</sup>, [M+2H]<sup>2+</sup>, and [M+3H]<sup>3+</sup> species from tryptic digests are given in parenthesis. Monoisotopic masses were derived from the flight times of features corresponding to the monoisotopic peaks using a calibration that was determined by electrospraying known solution mixtures (usually angiotensin II and individual tryptic digest mixtures). Estimated uncertainties in masses are ± 2.0 amu.

<sup>c</sup>Molecular weights correspond to the monoisotopic value for each peptide.

<sup>d</sup>Sequences expected from tryptic digestion of albumin (bovine and pig), cytochrome *c* (horse), and hemoglobin (dog and pig). Position of the peptide fragments within protein sequences is delineated by superscript numbers. An asterisk denotes those sequences that are observed in both the two-dimensional (Fig. 2) and three-dimensional experiments. Measures to reduce and alkylate disulfide bonds are not employed in these studies. Peptides containing cysteine residues, constituting a small portion of the total peptides, are tentatively assigned based on molecular weight.

<sup>e</sup>Proteins are labeled as al, cytc, and hb for albumin, cytochrome *c*, and hemoglobin, respectively. Within protein families, animal sources are separated with an underscore.

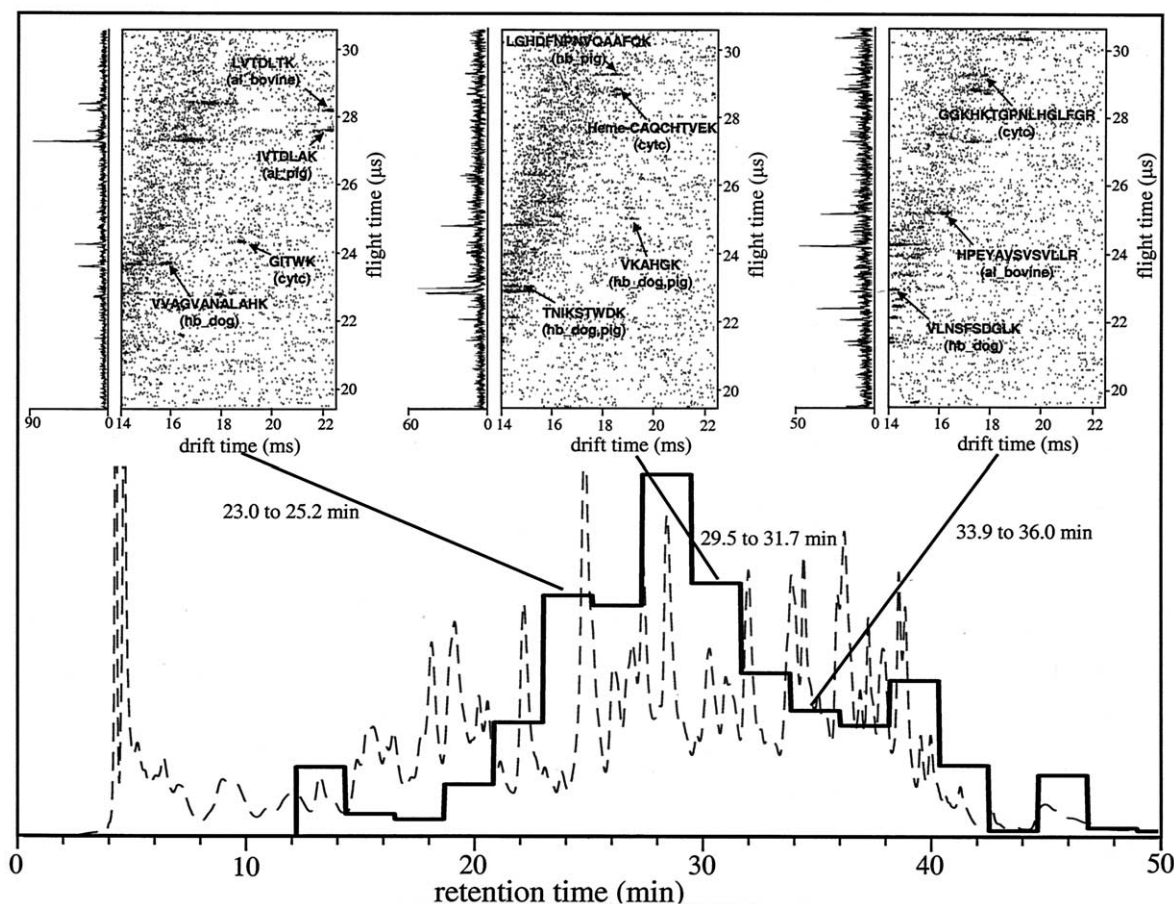


Fig. 3. Representation of multidimensional HPLC-IMS-MS separation for the mixture of peptides shown in the  $t_d(t_f)$  plot of Fig. 2. The solid horizontal and vertical steps represents the integrated ion intensity over the 14.0–22.5 ms drift time and 19.4–30.5  $\mu$ s ranges of the nested  $t_d(t_f)$  distributions. In order to illustrate the condensed-phase separation we have superimposed a plot of a HPLC separation (using a UV detection system) for the same mixture that was acquired in a separate experiment (dashed line). Three insets of nested  $t_d(t_f)$  datasets recorded over 23.0–25.2 (left), 29.5–31.7 (middle), and 33.9–36.0 min (right) are shown. Each inset (or step, along the retention time axis) is 127 s in duration and requires 3 s to save to the computer. During the 127 s timescale, the nested  $t_d(t_f)$  experiment is repeated 2540 times. The parameters associated with the ion mobility separation are the same as those in Fig. 2. The  $t_d(t_f)$  distributions are shown as point plots, where no cutoff was used. Thus, any  $t_d(t_f)$  window in which a single ion hit is recorded is displayed as a point. Several clusters of points are labeled with specific sequence assignments. Also shown to the left of each two-dimensional  $t_d(t_f)$  plot is a summed mass spectrum.

time axis we have displayed horizontal lines corresponding to the relative integrated ion intensities observed over the two dimensional  $t_d(t_f)$  windows. We have also shown an illustration of a typical HPLC separation (using a UV detector) of the mixture of peptide fragments that was recorded prior to the multidimensional data acquisition. The integrated ion intensities from the  $t_d(t_f)$  data generally track the profile of the UV trace; however, differences are

apparent - some due to variations between relative ionization efficiency and MS detection of components compared with absorbance. Over the ~12–55 min range where most peptides elute, only 20  $t_d(t_f)$  distributions (130 s in duration) are acquired, far less than the sampling rate required to accurately capture all of the distinct features that are resolved along the retention time axis.

The insets in Fig. 3 show examples of nested  $t_d(t_f)$

spectra acquired during three different ranges of retention times: 23.0–25.2; 29.5–31.7; and 33.9–36.0 min. All three of these  $t_d(t_p)$  distributions (and all of the others - not shown) differ substantially in appearance, as is expected. The nested  $t_d(t_p)$  windows appear much simpler and peaks are less congested than the data in Fig. 2; many peaks that would otherwise overlap along the mass axis are easily resolved based on the gas-phase separation. Analysis of all of the  $t_d(t_p)$  windows in the multidimensional dataset shows evidence for 183 unique peaks, substantially more than the 98 resolved peaks in the  $t_d(t_p)$  data shown in Fig. 2. Although we have resolved more peaks, we have only assigned 69 peaks to tryptic fragments (Table 1). The assigned sequences cover ~26.4%, 30.7%, 68.3%, 49.0%, and 59.5% of the total amino acid sequences for the albumin (bovine), albumin (pig), cytochrome c, hemoglobin (dog), and hemoglobin (pig) proteins, respectively.

The increased number of peaks in the three-dimensional dataset relative to the two-dimensional  $t_d(t_p)$  data (Fig. 2) probably arises because of differences in ionization efficiencies in the two experiments. When all components of the mixture are electrosprayed some components may be preferentially ionized - suppressing other peaks. The initial HPLC fractionation step provides a means of removing species that may interfere with the ionization process. It should be noted that other work on direct electrospray of mixtures of small peptides shows that at low concentrations matrix effects normally do not appear to obscure components [30,31]. We note that the number of resolved peaks in the three-dimensional experiment is also increased (relative to Fig. 2) because the reduction in spectral congestion also allows many more features to be easily resolved. Many of the peaks in the three-dimensional experiment do not correspond to tryptic fragments expected from complete protein digestion as well as those that arise from one or two missed cleavages. It is possible that some of these arise from a greater amount of incomplete protein digestion or from chymotryptic activity; however, an exhaustive comparison is not attempted here.

Although the percent sequence coverage increases

for four proteins, it actually decreases for pig hemoglobin (see previous) in the multidimensional experiment. As mentioned previously, the increase in sequence coverage may result from an increase in ionization efficiency for some peptides because of the removal of interfering species. Conversely, the ionization of certain species may be hampered by the solution conditions in the multidimensional experiment. For example, a high percentage of water is not as amenable to the electrospray process for the ESI source used in these studies; some species with smaller retention times may not be as easily observed in the multidimensional experiment. It should be noted that the increase in percent sequence coverage should not be the same for all proteins. For example, a protein that has a high-sequence coverage in the direct infusion experiment may not be expected to have as large an increase as a protein that has a small-sequence coverage initially due to fewer remaining peptides for the former. In addition, peptides produced from tryptic digestion of some proteins may have low ionization efficiencies and are therefore not observed in either experiment.

Perhaps the most useful illustration of the three-dimensional approach comes about from the ability to resolve components having mobilities and  $m/z$  ratios that were indistinguishable in the nested  $t_d(t_p)$  distribution shown in Fig. 2. We have noted previously that components in peak 1(y) are not entirely separated because of the similarities of mobilities and  $m/z$  ratios associated with three peptides (AACLLPK, NLDNLK, and VADALTK) that are expected to be formed by tryptic digestion of the proteins. Fig. 4 shows  $t_d(t_p)$  windows recorded at two different retention time intervals; these data allow unambiguous assignments of peak 1(y). During the 12.2–14.3 min retention window we observe a peak at  $m/z = 718.2$  - in good agreement with the calculated value of 717.4 for the  $[\text{VADALTK} + \text{H}]^+$  ion. During the 20.9–23.0 min window we observe two peaks having  $m/z = 717.4$  and 716.5. We assign these to the  $[\text{NLDLNK} + \text{H}]^+$  and  $[\text{AACLLPK} + \text{H}]^+$  ions having calculated  $m/z$  ratios of 716.4 and 715.4, respectively. Assignments of these peaks based on  $m/z$  comparison alone are not unambiguous because the

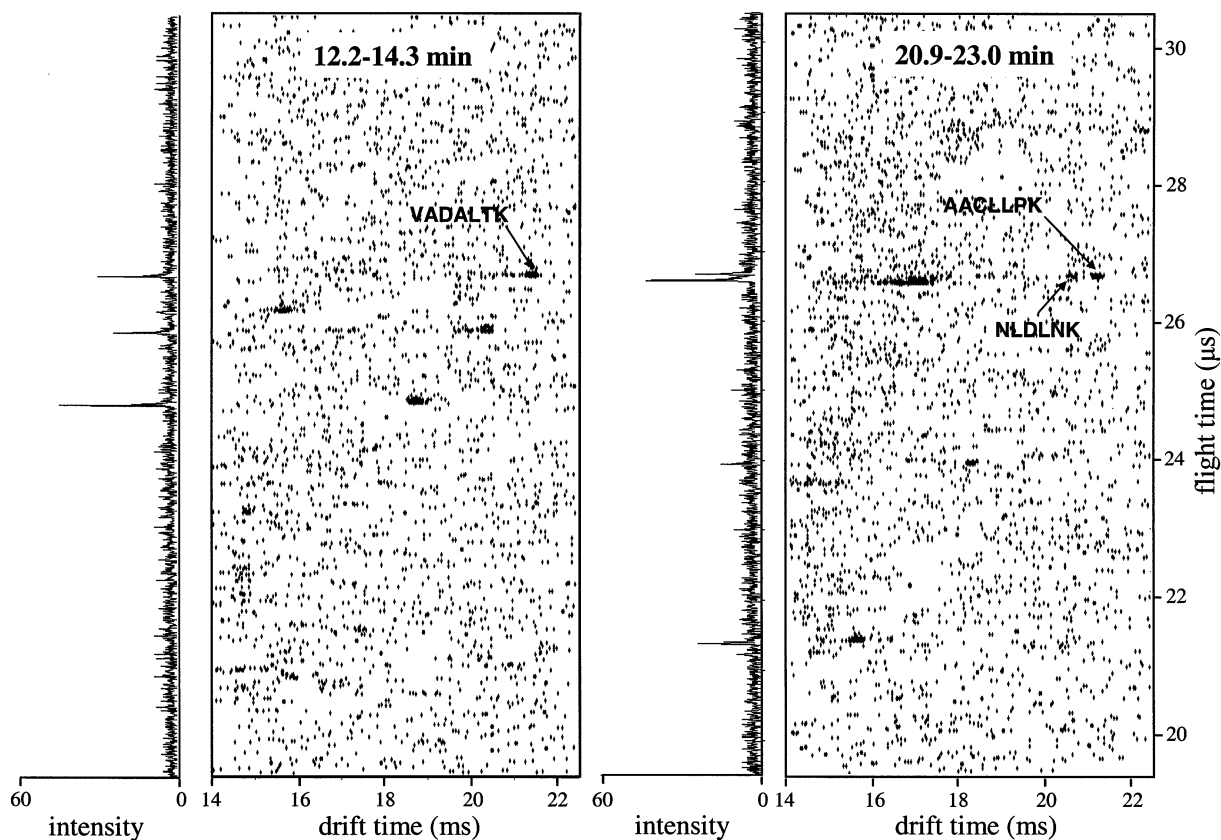


Fig. 4. Two dimensional point plots and summed mass spectra (left) acquired at retention time intervals of 12.2–14.3 (left) and 20.9–23.0 min (right). All experimental and plot parameters are identical to those discussed in Fig. 3. The three peptides (labeled in the figure) are resolved because of the HPLC separation. These peptides comprise the broad unresolved feature in Fig. 2 that is labeled 1(y).

comparisons are near the current mass accuracy of our  $m/z$  measurement. However, the mobilities of these three peptides have been measured previously and are in good agreement with the proposed  $m/z$ -based assignment. The ability to resolve and corroborate the assignment of peaks from mobility information emphasizes the importance of this dimension of separation. Table 1 shows two other similar examples of the advantages associated with the HPLC separation for unresolved peptides in peaks 2(1) and 2(t) of Fig. 2.

### 3.3. Assessment of two-dimensional and three-dimensional methods

It is instructive to consider the peak capacity afforded by the HPLC-IMS-TOFMS method and

address where improvements in this approach could be made. The peak capacity along a single dimension is usually defined in terms of the width of a peak at its base. It has been shown that peak capacity of a multidimensional approach is the product of the independent peak capacities along each dimension [11]. In our system the peak capacity of the LC dimension is the number of  $t_d(t_p)$  windows that were recorded during the timescale of the separation. We use a value of 20 since no useful data were acquired after HPLC retention times of  $\sim 55$  min [32]. Based on the resolving power of our mass spectrometer, we make a very conservative estimate of the peak capacity (over the  $m/z = 390$ – $920$  range) as  $\sim 400$ .

It is clear that the mass and mobility dimensions are correlated. Thus, the gain in peak capacity asso-

ciated with the ion mobility dimension is somewhat more difficult to assess. We can estimate theoretical limits for the gain in peak capacity associated with the ion mobility separation by considering the range of mobilities observed at a given mass and the instrumental resolving power. Families of +1 and +2 ions are usually well resolved. Within each of these families (at a given  $m/z$  ratio), mobilities vary by as much as  $\sim 20\%$ . Using typical values of  $t_d/\Delta t \approx 120$  to 150 for singly charged ions, we estimate the IMS peak capacity for peptides in the  $[M + H]^+$  family to be  $\sim 14$ –18. Taking into account that the ability to resolve ion mobility peaks increases in proportion to the square root of the ion charge [Eq. (1)], we calculate a peak capacity of  $\sim 20$ –25 for the +2 family. We estimate the peak capacity for ions in the +3 family as  $\sim 12$ –15, somewhat less than the +2 family because elongated +3 conformers can overlap with the +2 family peaks. We take the sum of these values,  $\sim 46$ –58, to be the peak capacity along the IMS dimension at any  $m/z$  value within the 390–920 range. The product of the peak capacities of the three separation dimensions gives the  $\sim 3.7$ – $4.6 \times 10^5$  value. The present methods appear to be useful for mixtures that are substantially more complex than the example shown here. We speculate that most components in mixtures containing a factor of ten more peptides would be resolvable.

There is clearly room for improving these methods. For example, our conservative estimate of a peak capacity of 400 for the MS dimension is much less than values that are attainable by high-resolution TOF methods. The resolving power along the MS dimension of our instrument is currently limited by use of a relatively long 5 ns window—a compromise that reduces the total size of the  $t_d(t_p)$  array. We are currently developing a new acquisition system to improve the MS resolving power.

A significant limitation in the total peak capacity arises because of the time required to record  $t_d(t_p)$  windows along the retention time dimension. This limitation is largely due to the relatively low ion signals in these experiments (compared with LC-MS). Drift tube experiments involving a continuous ion source such as ESI are intrinsically inefficient because

of limitations associated with the requirement of an initial short pulse of ions and because ions drift across the instrument, they diffuse such that only a limited fraction exit the drift tube. Advances in ion trapping and focusing methods at high pressures would allow  $t_d(t_p)$  windows to be recorded rapidly; improvements in sampling would increase the peak capacity along the LC dimension. Additionally it would allow the two dimensional approach to be coupled with other condensed phase separation methods.

#### 4. Summary and conclusions

A multidimensional separation strategy in which HPLC is combined with high resolution IMS and TOFMS has been described. In this approach, components in a mixture are separated using reversed phase HPLC. As mixtures of eluents exit the column, they are electrosprayed into the gas phase and 25 nested  $t_d(t_p)$  distributions (each 130 s in duration) have been recorded. The combined retention-, drift-, and flight-time data form the basis of the three dimensional separation. The approach is feasible because of the large differences in timescales of the HPLC (minutes), ion mobility (milliseconds), and time-of-flight MS (microseconds) techniques.

The method is demonstrated for a mixture of peptides generated by tryptic digestion of five common proteins: albumin, bovine and pig; cytochrome c; hemoglobin, dog and pig. Complete digestion of these proteins is expected to produce 187 fragments. Of these, 145 are expected to form either  $[M + H]^+$  or  $[M + 2H]^{2+}$  ions that will be observed over the  $m/z = 390$ –920 range studied here. Two-dimensional  $t_d(t_p)$  datasets (where no HPLC separation is used) show 98 peaks; many expected fragments,  $\sim 23.7\%$ ,  $14.8\%$ ,  $51.0\%$ ,  $39.0\%$ , and  $60.3\%$  of the total sequences for the albumin (bovine), albumin (pig), cytochrome c, hemoglobin (dog), and hemoglobin (pig) proteins, respectively, have been assigned. The multidimensional HPLC-IMS-MS method resolves 183 peaks for this mixture and  $\sim 26.4\%$ ,  $30.7\%$ ,  $68.3\%$ ,  $49.0\%$ , and  $59.5\%$  of the total sequences of these respective proteins are observed. The ability to

examine smaller fractions of the mixture as peptides elute from the column makes it possible to resolve some fragments that could not be resolved in the two-dimensional  $t_d(t_f)$  dataset. An example in which three peptides, AACLLPK, NLDNLK, and VADALTK (having nearly identical  $m/z$  ratios and mobilities) could be easily distinguished in the multidimensional approach is presented.

Although a limited  $m/z$  range (390–920) is used in these studies, we have identified peptides of vastly different sizes - from 3 to 24 residues (Table 1). The mobility separation facilitates this by separating ions into charge state families prior to MS analysis. Thus, most of the information about the digest can be distinguished even over a relatively narrow range.

In order to assess the utility of the approach we have estimated peak capacities of  $\sim 900$ – $1200$  for the two-dimensional LC-IMS and  $\sim 3.7$ – $4.6 \times 10^5$  for the three-dimensional LC-IMS-MS separations, respectively. Higher values would be obtained by improving peak capacities along any of the individual dimensions. We estimate that inclusion of high-resolution ion mobility separations between other existing methods could increase peak capacities by factors of  $\sim 46$ – $58$  across a distribution of +1, +2, and +3 ions. Currently the timescale required for acquisition of sequential nested  $t_d(t_f)$  datasets during the LC separation introduces a significant sampling limitation. The net result is that currently the peak capacity along the HPLC dimension is substantially below the value that would otherwise be accessible using this method. We are currently implementing methods to improve ion transmission through the drift tube [33].

Sampling limitations arise because of relatively low signal in these experiments. The continuous nature of ESI and the requirement of pulses for the ion mobility measurements result in an inefficient coupling. It is typical to discard 99%–99.9% of the ion signal during the mobility experiment [34]; thus, these experiments are inherently less sensitive than conventional LC-ESI-MS methods. We have recently shown that an ion trap interface can be used to accumulate  $\sim 70\%$ – $100\%$  of ions between ion mobility pulses [34]; however, whereas this configuration is useful for an injected ion drift tube configuration, it currently

cannot be implemented at high pressures. We are working on several methods to trap ions at high pressures in order to improve the efficiencies of the present techniques. Such improvements should make it possible to acquire nested  $t_d(t_f)$  data during much shorter windows, improving sampling and peak capacities along the condensed phase separation axis. This would allow these methods to be coupled with higher-resolution condensed phase techniques such as charge exchange. Additionally, four-dimensional separations, involving either a two-dimensional condensed phase separation [12] coupled with  $t_d(t_f)$  detection, or an LC-IMS-tandem mass spectrometry analysis should also be possible. We are currently developing an instrument to investigate the latter method [35].

## Acknowledgements

This work was supported in part by grants from the National Institutes of Health (1R01 GM59145-01 and 55647-03) and research awards from the Sloan and Dreyfus foundations.

## References

- [1] C.S. Hoaglund, S.J. Valentine, C.R. Sporleder, J.P. Reilly, D.E. Clemmer, *Anal. Chem.* 70 (1998) 2236.
- [2] G.R. Asbury, C. Wu, W.F. Siems, H.H. Hill, Pittcon, New Orleans, LA, 1998, oral presentation of abs. 568.
- [3] G. von Helden, M.T. Hsu, P.R. Kemper, M.T. Bowers, *J. Chem. Phys.* 95 (1991) 3835.
- [4] G. von Helden, M.-T. Hsu, N. Gotts, M.T. Bowers, *J. Phys. Chem.* 97 (1993) 8182.
- [5] K.B. Shelimov, J.M. Hunter, M.F. Jarrold, *Int. J. Mass Spectrom. Ion Processes* 138 (1994) 17; J.M. Hunter, M.F. Jarrold, *J. Am. Chem. Soc.* 117 (1995) 10317.
- [6] C.A. Srebalus, J. Li, W.S. Marshall, D.E. Clemmer, *Anal. Chem.* 71 (1999) 3918.
- [7] S.J. Valentine, A.E. Counterman, C.S. Hoaglund, J.P. Reilly, D.E. Clemmer, *J. Am. Soc. Mass Spectrom.* 9 (1998) 1213.
- [8] S.J. Valentine, A.E. Counterman, C.S. Hoaglund-Hyzer, D.E. Clemmer, *J. Phys. Chem.* 103 (1999) 1203.
- [9] S.C. Henderson, S.J. Valentine, A.E. Counterman, D.E. Clemmer, *Anal. Chem.* 71 (1999) 291.
- [10] S.J. Valentine, A.E. Counterman, D.E. Clemmer, *J. Am. Soc. Mass Spectrom.* 10 (1999) 1188.

- [11] J.C. Giddings, J. High Resolut. Chromatogr. Chromatogr. Commun. 10 (1987) 319.
- [12] M.M. Bushey, J.W. Jorgenson, Anal. Chem. 62 (1990) 978; M.M. Bushey, J.W. Jorgenson, J. Microcolumn Sep. 2 (1990) 293.
- [13] D.F. Hunt, R.A. Henderson, J. Shabanowitz, K. Sakaguchi, M. Michel, N. Sevilir, A. Cox, E. Appella, V.H. Engelhard, Science 255 (1992) 1261.
- [14] D.F. Hunt, J.E. Alexander, A.L. McCormack, P.A. Martino, H. Michel, J. Shabanowitz, N. Sherman, M.A. Moseley, J.W. Jorgenson, K.B. Tomer, in Techniques in Protein Chemistry II, J.J. Villafranca (Ed.), Academic, New York, 1992, p. 441.
- [15] C.G. Edmonds, J.A. Loo, H.R. Barnaga, H.R. Udseth, R.D. Smith, J. Chromatogr. 474 (1989) 21; M.A. Moseley, J.W. Jorgenson, J. Shabanowitz, D.F. Hunt, K.B. Tomer, J. Am. Soc. Mass Spectrom. 3 (1992) 289; S. Pleasance, P. Thibault, in Capillary Electrophoresis: Theory and Practice, P. Camilleri, (Ed.), CRC, Boca Raton, 1993, p. 311.
- [16] G.A. Valaskovic, N.L. Kelleher, F.W. McLafferty, Science 273 (1996) 1199.
- [17] P.K. Jensen, L. Pasa-Tolic, G.A. Anderson, J.A. Horner, M.S. Lipton, J.E. Bruce, R.D. Smith, Anal. Chem. 71 (1999) 2076; H.Y. Gao, Y.F. Shen, T.D. Veenstra, R. Harkewicz, G.A. Anderson, J.E. Bruce, L. Pasa-Tolic, R.D. Smith, J. Microcolumn Sep. 12 (2000) 383; W. Li, C.L. Hendrickson, M.R. Emmett, A.G. Marshall, Anal. Chem. 71 (1999) 4397; S.E. Martin, J. Shabanowitz, D.F. Hunt, J.A. Marto, Anal. Chem. 72 (2000) 4266.
- [18] D.F. Hagen, Anal. Chem. 51 (1979) 870; J.C. Tou, G.U. Boggs, Anal. Chem. 48 (1976) 1351; R.H. St. Louis, H.H. Hill, Crit. Rev. Anal. Chem. 21 (1990) 321; H.H. Hill, W.F. Siems, R.H. St. Louis, D.G. McMinn, Anal. Chem. 62 (1990) 1201A; G. von Helden, M.T. Hsu, P.R. Kemper, M.T. Bowers, J. Chem. Phys. 95 (1991) 3835; Z. Karpas, Stimac, Z. Rappaport, Int. J. Mass Spectrom. Ion Processes 83 (1988) 163; M.F. Jarrold, J. Phys. Chem. 99 (1995) 11.
- [19] D.E. Clemmer, M.F. Jarrold, J. Mass Spectrom. 32 (1997) 577; Y. Liu, S.J. Valentine, A.E. Counterman, C.S. Hoaglund, D.E. Clemmer, Anal. Chem. 69 (1997) 728A; M.F. Jarrold, Acc. Chem. Res. 32 (1999) 360; C.S. Hoaglund-Hyzer, A.E. Counterman, D.E. Clemmer, Chem. Rev. 99 (1999) 3037.
- [20] T. Wyttbach, G. von Helden, M.T. Bowers, J. Am. Chem. Soc. 118 (1996) 8355; T. Wyttbach, J.E. Bushnell, M.T. Bowers, *ibid.*, 120 (1998) 5098.
- [21] D.E. Clemmer, R.R. Hudgins, M.F. Jarrold, J. Am. Chem. Soc. 117 (1995) 10141; K.B. Shelimov, M.F. Jarrold, *ibid.*, 119 (1997) 2987; K.B. Shelimov, D.E. Clemmer, R.R. Hudgins, M.F. Jarrold, *ibid.*, 119 (1997) 2240; R.R. Hudgins, M.A. Ratner, M.F. Jarrold, *ibid.*, 120 (1998) 12974; R.R. Hudgins, Y. Mao, M.A. Ratner, M.F. Jarrold, Biophys. J. 76 (1999) 1591.
- [22] S.J. Valentine, D.E. Clemmer, J. Am. Chem. Soc. 119 (1997) 3558; S.J. Valentine, J. Anderson, A.E. Ellington, D.E. Clemmer, J. Phys. Chem. B 101 (1997) 3891; S.J. Valentine, A.E. Counterman, D.E. Clemmer, J. Am. Soc. Mass Spectrom. 8 (1997) 954.
- [23] C. Wu, W.F. Siems, G.R. Asbury, H.H. Hill, Anal. Chem. 70 (1998) 4929; C. Wu, J. Klasmeier, H.H. Hill, Rapid Commun. Mass Spectrom. 13 (1999) 1138.
- [24] No purity information is given for these proteins.
- [25] A.E. Counterman, S.J. Valentine, C.A. Srebalus, S.C. Henderson, C.S. Hoaglund, D.E. Clemmer, J. Am. Soc. Mass Spectrom. 9 (1998) 743.
- [26] H.W. Revercomb, E.A. Mason, Anal. Chem. 47 (1975) 970.
- [27] P. Dugourd, R.R. Hudgins, D.E. Clemmer, M.F. Jarrold, Rev. Sci. Instrum. 68 (1997) 1122.
- [28] D.A. Skoog, J.J. Leary, Principles of Instrumental Analysis, Fourth Ed., Saunders College Publishing, New York, 1992, p. 587.
- [29] MATLAB Version 4, The Math Works, Inc., Natick, MA, 1997.
- [30] J.L. Stephenson, S.A. McLuckey, J. Am. Soc. Mass Spectrom. 9 (1998) 585.
- [31] C.A. Srebalus, J. Li, W.S. Marshall, D.E. Clemmer, J. Am. Soc. Mass Spectrom. 11 (2000) 352.
- [32] Improvements in the ion signal should allow substantially higher sampling rates and higher peak capacities.
- [33] Y.J. Lee, C.S. Hoaglund-Hyzer, J.A. Taraszka, G.A. Zientara, A.E. Counterman, D.E. Clemmer, Anal. Chem. 73 (2001) 3549.
- [34] C.S. Hoaglund, S.J. Valentine, D.E. Clemmer, Anal. Chem. 69 (1997) 4156.
- [35] C.S. Hoaglund-Hyzer, J. Li, D.E. Clemmer, Anal. Chem. 72 (2000) 2737; C.S. Hoaglund-Hyzer, D.E. Clemmer, Anal. Chem. 73 (2001) 177.